Applied Catalysis A: General 431–432 (2012) 104–112

Contents lists available at SciVerse ScienceDirect

Applied Catalysis A: General

journal homepage: www.elsevier.com/locate/apcata

Interaction of Zn^{2+} with extraframework aluminum in HBEA zeolite and its role in enhancing *n*-pentane isomerization

Nur Hidayatul Nazirah Kamarudin[a], Aishah Abdul Jalil[a], Sugeng Triwahyono[b,*], Rino R. Mukti[c], Muhammad Arif Ab Aziz[a], Herma Dina Setiabudi[a], Mohd Nazlan Mohd Muhid[d], Halimaton Hamdan[d]

[a] *Institute of Hydrogen Economy, Faculty of Chemical Engineering, Universiti Teknologi Malaysia, 81310 UTM Johor Bahru, Johor, Malaysia*
[b] *Ibnu Sina Institute for Fundamental Science Studies, Faculty of Science, Universiti Teknologi Malaysia, 81310 UTM Johor Bahru, Johor, Malaysia*
[c] *Division of Inorganic and Physical Chemistry, Faculty of Mathematics and Natural Science, Institut Teknologi Bandung, Jl Ganesha No 10, Bandung 40132, Indonesia*
[d] *Department of Chemistry, Faculty of Science, Universiti Teknologi Malaysia, 81310 UTM Johor Bahru, Johor, Malaysia*

ARTICLE INFO

Article history:
Received 25 February 2012
Received in revised form 9 April 2012
Accepted 15 April 2012
Available online 1 May 2012

Keywords:
Zn-HBEA
Extraframework aluminum
Bridging hydroxyl groups
Protonic acid sites
n-Pentane isomerization

ABSTRACT

The electrodeposition method was used to produce Zn^{2+} cation precursors, followed by the introduction of Zn^{2+} cation precursors to HBEA by the ion exchange technique. The introduction of Zn^{2+} cations slightly changed the specific surface area and crystallinity of HBEA. IR, XPS and solid state MAS NMR results showed that Zn^{2+} cations interacted with $(AlO)^+$ extraframework aluminum to form $Zn(OAl{=})_2$ and simultaneously induced the formation of bridging hydroxyl groups, Si(OH)Al. The pyridine adsorbed IR study revealed that the presence of Zn^{2+} cations fully eliminated weak and partially eliminated strong Brønsted acid sites. As a result, strong and relatively weak Lewis acid sites were formed in which the pyridine probe molecule desorbed at 623 K and below. The presence of Zn^{2+} cations enhanced the catalytic activity of HBEA in *n*-pentane isomerization due to the presence of strong Lewis acid sites; the sites may facilitate the formation and maintenance of active protonic acid sites through a hydrogen spillover mechanism. At 598 K, the yield of isopentane for Zn-HBEA was 25.7% higher than that of HBEA. Within a reaction temperature range of 373–648 K, the apparent activation energy for isomerization of *n*-pentane over HBEA and Zn-HBEA was 118.76 and 90.79 kJ/mol, respectively.

1. Introduction

Hydroisomerization of paraffins to enhance the octane number of gasoline is an environmentally more acceptable method compared to other technologies such as blending with oxygenates like MTBE, which has been identified as a source of groundwater contamination. It is clear that branched paraffins are the preferred gasoline component; therefore, it is highly desirable to increase the contribution of high octane branched paraffins to the gasoline pool [1]. Alkane isomerization is typically carried out over bifunctional metal-acid catalysts [2] and it is well established that the isomerization proceeds through consecutive branching reactions. Isomerization takes place at the acid sites of the bifunctional catalyst, whereas the metal site provides hydrogenation–dehydrogenation capability. Several types of solid acid catalyst such as MOR [3], SAPO-11 [4], ZSM-22 [5], ZSM-5 [6,7], Beta [8,9], HY [10,11] and oxoanions loaded on ZrO_2 [2,12–14] have been used for the isomerization process. The addition of noble or transition metals to catalysts and the presence of hydrogen in the gas phase markedly improve the activity and stability of the catalyst. Transition metals such as platinum, zinc and iridium cations loaded on support catalysts have also been reported to improve the production of isoproducts and to suppress the cracking reaction in *n*-heptane isomerization over Pt/HY zeolite [7,15,16]. These cationic transition metals might play an important role in speeding up the desorption of olefinic species from the surface of the catalyst, thereby preventing the secondary reaction and/or thermal decomposition of reactants and products.

Particularly, the roles of Zn metal in solid catalysts have been discussed by several research groups in recent years. Saberi et al. reported on *n*-heptane isomerization over Pt–Zn–HY trifunctional catalysts in which they concluded that each reaction temperature needs a specific Zn loading in order to obtain the maximum activity for isomerization [9]. Freude and co-workers explored the properties of Zn/H–BEA zeolite by ^{1}H MAS NMR and IR spectroscopy of adsorbed CO [17,18]. Kazansky et al. reported that Zn^{2+} ions introduced into ZSM-5 zeolites resulted in the partial localization of Zn^{2+} ions at negatively charged tetrahedral AlO_4^-, which led to a partial decrease in the Brønsted acidic sites and obstruction of the remaining bridging OH groups [19]. This factor led to a considerable suppression of the cracking activity of zeolites which certainly needs proton donor centers. An extension of the study

* Corresponding author. Tel.: +60 7 5536076; fax: +60 7 5536080.
E-mail addresses: sugeng@utm.my, sugengtw@gmail.com (S. Triwahyono).

0926-860X/$ – see front matter © 2012 Elsevier B.V. All rights reserved.
http://dx.doi.org/10.1016/j.apcata.2012.04.020

established that ion exchange and impregnation of Zn species on ZSM-5 decreased the intensity of the band of bridging hydroxyl groups (3610 cm^{-1}). In addition, a shoulder band at 3660 cm^{-1} assigned to basic $(ZnOH)^+$ groups was also observed. Nevertheless, Biscardi et al. [20] reported, using X-ray absorption data, that $(ZnOH)^+$ species are not thermally stable and easily undergo dehydration by coupling of $(ZnOH)^+$ species with acidic OH groups to form water and a bridging Zn^{2+} cation that interacts with bridging hydroxyl groups, Si(OH)Al. This type of exchanged zinc was found to increase propane conversion turnover rates, hydrogen formation rates and selectivity to aromatics on H-ZSM5. Our research group has recently reported the positive effect of zinc on HZSM-5 in the isomerization of *n*-pentane [21]. Similarly, Zn^{2+} ions interacted with acidic hydroxyl groups, Si(OH)Al at 3610 cm^{-1} to form Lewis acid sites ($Zn^{2+}(O^-)_2$).

Based on several previous reports, most of the Zn species interacts with bridging hydroxyl groups, Si(OH)Al, to change the acidic character of the sample. However, no detailed study in the literature has been reported on the interaction of Zn species with non-bridging hydroxyl groups. Thus, in this study, we have endeavored to introduce Zn^{2+} cations into HBEA in which the HBEA possesses no acidic bridging hydroxyl groups after calcination at 1023 K. The IR, XPS and solid state MAS NMR results confirmed that Zn^{2+} cations interact with acidic sites corresponding to the $(AlO)^+$ extraframework aluminum to generate strong Lewis acid sites and simultaneously develop bridging hydroxyl groups, Si(OH)Al. The effect of Zn^{2+} in *n*-pentane catalytic isomerization over HBEA will also be discussed.

2. Experimental

Zn^{2+}/DMF solution was used as a Zn^{2+} cation precursor and was prepared as follows [22]. In brief, a DMF solution (Merck) containing naphthalene and tetraethylammonium perchlorate (TEAP) was added in a single-compartment cell fitted with a zinc plate as the anode and a platinum plate as the cathode. The electrodeposition of Zn^{2+} cation was done at 273 K. The protonated BEA zeolite (HBEA) was obtained by calcination of ammonium-exchanged BEA zeolite with an Si/Al ratio of 75 (Zeolyst International) at 1023 K for 3 h with a heating rate of 3 K/min. The zinc-loaded HBEA (Zn-HBEA) was prepared by ion exchange of HBEA with Zn^{2+}/DMF solution at room temperature for 4 h. The product was then filtered, followed by drying at 383 K for 12 h and calcination at 823 K for 3 h. The AAS analysis confirmed that the amount of Zn was 0.3 wt%.

The crystallinity of catalysts was measured with a Bruker Advance D8 X-ray powder diffractometer with Cu Kα (λ = 1.5418 Å) radiation as the diffracted monochromatic beam at 40 kV and 40 mA. X-ray photoelectron spectroscopy (XPS) of Zn-HBEA was conducted using a Kratos Ultra spectrometer with a Mg Kα radiation source (10 mA, 15 kV) and the XPS peaks were internally referenced to the binding energy of the C (1s) peak at 284.5 ± 0.1 eV. Nitrogen physisorption analysis was conducted on a Quantachrome Autosorb-1 at 77 K. Before the measurement, the sample was evacuated at 573 K for 3 h. Infrared (IR) measurements were carried out using a PerkinElmer Spectrum GX FT-IR spectrometer. IR spectra were recorded on a transmission spectrometer in which the sample was prepared as a self-supporting wafer and activated under vacuum at 673 K for 3 h in accordance with a previous report [23]. The adsorption of pyridine (2 Torr) was carried out at 423 K for 30 min, followed by outgassing at 423, 523 and 623 K for 30 min. In order to determine the amount of coke deposits, thermogravimetric analysis (TGA) was conducted using a Mettler Toledo TGA/SDTA 851. Temperature was programmed from ambient temperature to 1173 K at a heating rate of 10 K/min under N_2 flow.

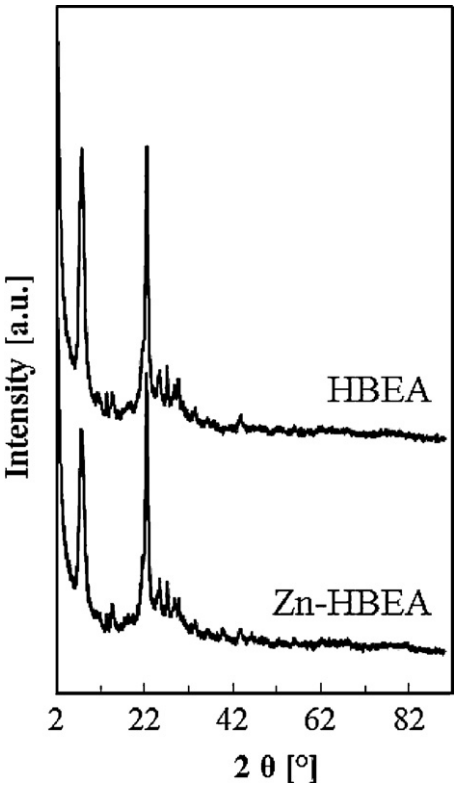

Fig. 1. XRD patterns of HBEA and Zn-HBEA.

Hydroisomerization of *n*-pentane was carried out under atmospheric pressure in a microcatalytic pulse reactor equipped with an online sampling valve for gas chromatographic analysis. About 0.2 g of the catalyst was placed in an ID 10 mm quartz glass reactor. Prior to the reaction, the catalyst was subjected to H_2 reduction at 723 K. A dose of *n*-pentane (0.5 μL) was injected over the catalyst at 598 K and the products were trapped at 77 K before flushing out to the gas chromatograph. The reaction products were analyzed by online 6090N Agilent Gas Chromatograph equipped with a VZ-7 packed column and an FID detector [23]. The intervals between each pulse injection were kept constant at 15 min. In order to observe the appropriate condition of *n*-pentane isomerization, the sample was reduced at different temperatures (598, 648, 673 and 723 K). The effects of the reaction temperature were observed at 593, 598, 603, 608 and 623 K.

3. Results and discussion

3.1. Characterization of catalysts

The crystallinity of catalysts was determined by comparing two major diffraction peaks of the samples. XRD peaks for both HBEA and Zn-HBEA were observed at 2θ = 7.8°, 16.5°, 21.5°, 22.5°, 25.3°, 27.1°, 29.6° and 43.5° in which these BEA phase peaks were similar to those reported by Higgins et al. [24] and Pariente et al. [25]. The peaks of Zn-HBEA apparently resembled the peaks of HBEA, although they differed in intensity (Fig. 1). Particularly, the intensity of the peak at 2θ = 7.8° decreased slightly upon the incorporation of Zn^{2+} cations. The decrease in the crystallinity was not due to the collapse of the framework structure of HBEA, but was rather due to the presence of Zn^{2+} cations on the external surface of HBEA. No diffraction peaks of ZnO crystallites (JCPD = 31.6°, 34.2°, 36.1°, 56.6°) in Zn-HBEA were observed, indicating that the Zn^{2+} cations species in the samples was highly dispersed on the surface of the zeolites. The effects of metal addition on zeolitic materials have

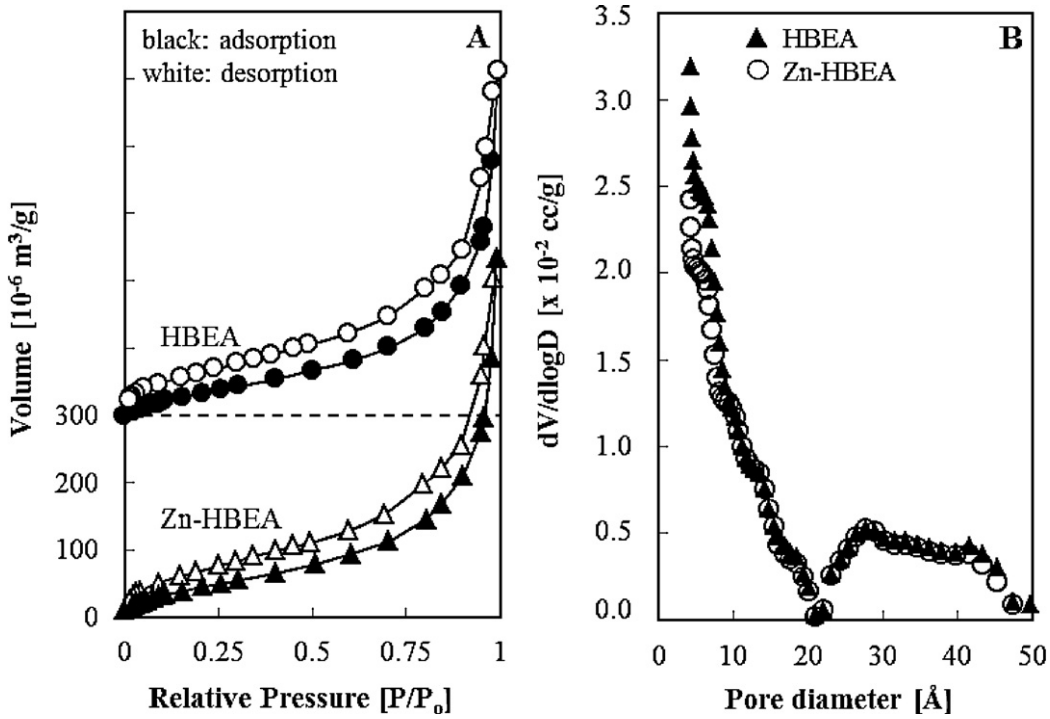

Fig. 2. (A) Nitrogen adsorption and desorption isotherms at 77 K for HBEA and Zn-HBEA. (B) Pore size distribution of HBEA and Zn-HBEA.

been reported by several research groups. Liu et al. reported the effect Cr, La, Ce and Zn on the Pt/HBEA in which the diffraction curves of all samples were almost identical to those of the parent sample HBEA, indicating highly comparable crystallinity and crystal structure of the BEA zeolite phase after loading of the metals [26]. Kumar et al. reported on the isomorphous substitution of Fe for Al on BEA zeolite in which the presence of Fe expanded the lattice size of zeolite due to the larger size of the Fe atom [27]. The collapse of the framework structure of Na–Y zeolite due to the interaction of Zn^{2+} cations in the lattice of the zeolite was demonstrated by Beyer and Keindl [28], whereas Ni et al. reported that the presence of Zn in the preparation of ZSM-5 hindered the crystallization of ZSM-5 [29].

The N_2 adsorption–desorption isotherms of the samples are shown in Fig. 2A. Both catalysts exhibited an isotherm similar to Type IV with a Type H4 hysteresis loop. At higher relative pressure

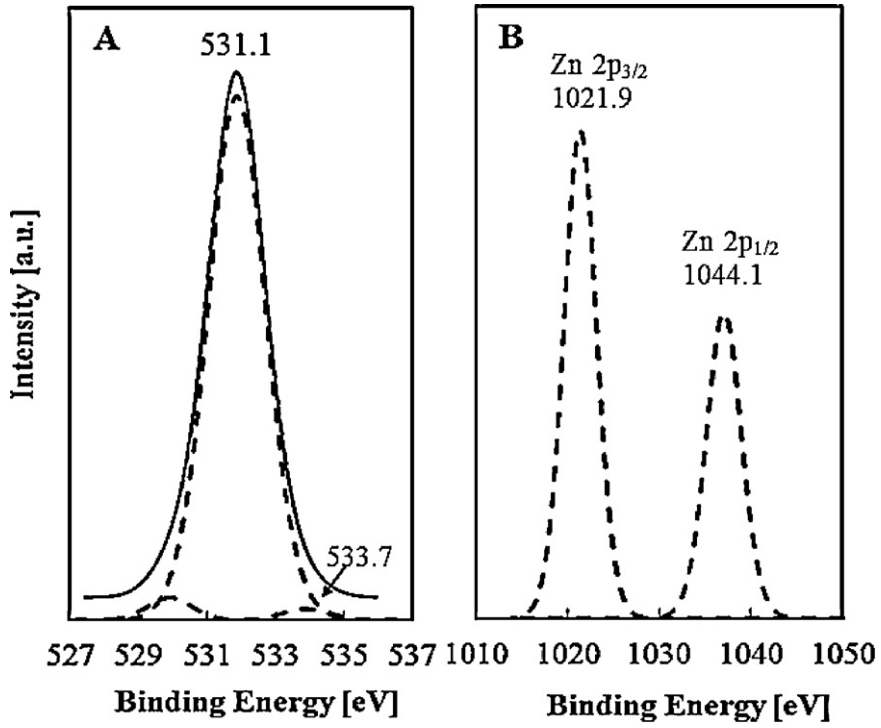

Fig. 3. XPS spectra of Zn-HBEA (A) O 1s and (B) Zn 2p.

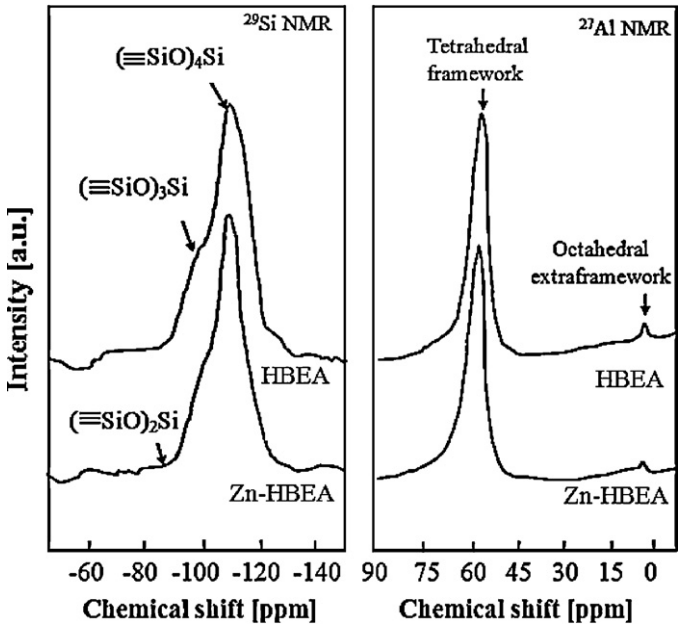

Fig. 4. ^{27}Al and ^{29}Si MAS NMR spectra of HBEA and Zn-HBEA.

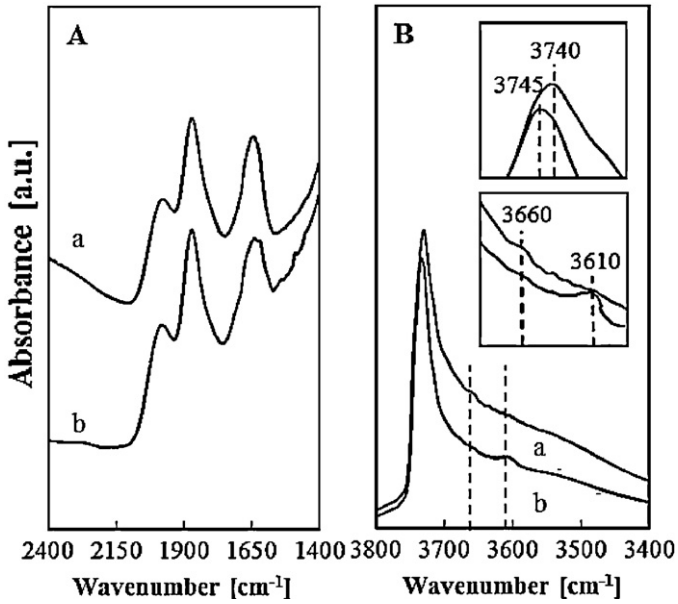

Fig. 5. IR spectra of HBEA and Zn-HBEA in the range of (A) 2400–1400 cm^{-1} and (B) 3800–3400 cm^{-1}.

(P/P_o between 0.8 and 1.0), a notable increase of adsorbed nitrogen was observed, suggesting an important external surface area contribution. The Type IV-like patterns of all samples are common isotherms given by adsorbents which possess mesopore structures, such as many silica gels and other porous oxides [30]. For both samples, desorption was at first gradual but suddenly became much more rapid at a relative pressure of about 0.8, while the desorption boundary curve did not converge to the adsorption isotherm. According to Sing, hysteresis of this type is often observed in measurements of nitrogen sorption in mesoporous solids [30]. A small change in the specific surface area was observed for Zn^{2+} cation-loaded HBEA; the specific surface areas of HBEA and Zn-HBEA were 558 and 544 m^2/g, respectively. The pore size distribution curve showed that introduction of Zn^{2+} cations plugs HBEA at a pore diameter around 4.17–7.84 and 41.5–47.5 Å (Fig. 2B).

The X-ray photoelectron spectroscopy (XPS) results confirmed the presence of Zn^{2+} and the absence of zinc metal and ZnO. Fig. 3 shows that the XPS peaks at 1021.9 and 1044.1 eV are due to the $Zn2p_{3/2}$ and $Zn2p_{1/2}$ energy levels, respectively. Both of these were symmetrical and narrow, showing the single charge state of Zn. According to Fig. 3A, the strong peak at 531.1 eV is assigned to the O atoms in the bulk, while the shoulder at 533.7 is attributed to OH groups at the Zn—O (0 0 0 1) surface [31]. A similar observation was obtained in our previous study for the introduction of Zn to HZSM-5, which verified the presence of Zn^{2+} cations on the zeolite surface [21].Fig. 4 shows the ^{29}Si and ^{27}Al MAS NMR spectra for the HBEA and Zn-HBEA samples. For ^{29}Si MAS NMR, both HBEA and Zn-HBEA samples showed a dominant peak at −111 ppm assigned to silicon atoms at the Q^4 site $(\equiv SiO)_4Si$ and a shoulder peak at −98 ppm assigned to silicon atoms at the Q^3 site $(\equiv SiO)_3Si$ [32]. A small and broad peak was observed in the range of −117 to −135 ppm for HBEA which may be attributed to the existence of crystallographically unequivalent sites in the sample, and very broad peak was observed at −89 ppm for Zn-HBEA which was assigned to silicon atoms at the Q^2 site $(\equiv SiO)_2Si$ [33]. The presence of Zn^{2+} slightly decreased the peak at −98 ppm, eliminated the peak at −117 to −135 ppm and developed a new peak at −89 ppm, whereas the presence of Zn^{2+} did not change the peak of ^{27}Al MAS NMR. Both samples consisted of an intense peak at 56 ppm and a small peak at 1 ppm indicative of the presence of tetrahedral and octahedral aluminums. These ^{29}Si and ^{27}Al MAS NMR results revealed that the presence of Zn^{2+}did not change the aluminum framework; however, it partially converted $(\equiv SiO)_3Si$ to $(\equiv SiO)_2Si$ and eliminated crystallographically unequivalent sites in the HBEA sample.Fig. 5 shows the FTIR spectra of activated HBEA and Zn-HBEA samples in the lattice and hydroxyl groups stretching regions. The spectra for the vibrational lattice stretching frequency was observed in the range of 1400–2400 cm^{-1} and the hydroxyl groups region was observed at 3400–3800 cm^{-1}. Referring to Fig. 5A, no significant change was observed on the vibrational lattice stretching frequency in the region of 2200–1750 cm^{-1}. This result resembled the XRD result in which Zn^{2+} did not change or destroy the lattice structure or crystallinity of HBEA. For hydroxyl group stretching regions, the absorbance bands were observed at 3740, 3660, 3610 and 3520 cm^{-1} (Fig. 5B). The band at 3740 cm^{-1} usually belongs to terminal SiOH groups on the external surface. The band at 3610 cm^{-1} is due to strongly acidic bridging hydroxyl groups; this band was not observed in the HBEA sample after high temperature calcination [34]. The broad and very weak band at 3520 cm^{-1} is assigned to bridging hydroxyls which are perturbed by H-bond interactions with the zeolitic framework [35]. The signal at 3660 cm^{-1} belongs to the acid OH groups connected to Al partially attached to the framework and located at the external surface. The presence of Zn^{2+} shifted the peak from 3740 cm^{-1} to 3745 cm^{-1}, indicating the formation of hydroxyl groups corresponding to the terminal and internal framework defect SiOH groups [17]. This result is in accordance with ^{29}Si MAS NMR results for the formation of silicon atoms at the Q^2 site. The elimination of the peak at 3660 cm^{-1} and the development of the peak at 3610 cm^{-1} indicated the interaction of Zn^{2+} with acidic hydroxyl groups corresponding to $(AlO)^+$ extraframework aluminum to form $Zn(OAl=)_2$, leaving OH groups. Then, the remaining OH groups reacts with the aluminosilicate framework to form bridging hydroxyl groups, Si(OH)Al and geminal silanol groups, $Si(OH)_2$. No change was observed for ^{27}Al MAS NMR, indicating that the formed $Zn(OAl=)_2$ is not attached to the aluminosilicate framework. Scheme 1 shows the possible mechanism for the interaction of Zn^{2+} with extraframework aluminum on the surface of HBEA.

On the contrary, several research groups have reported the interaction of Zn^{2+} with bridging hydroxyl groups in the framework

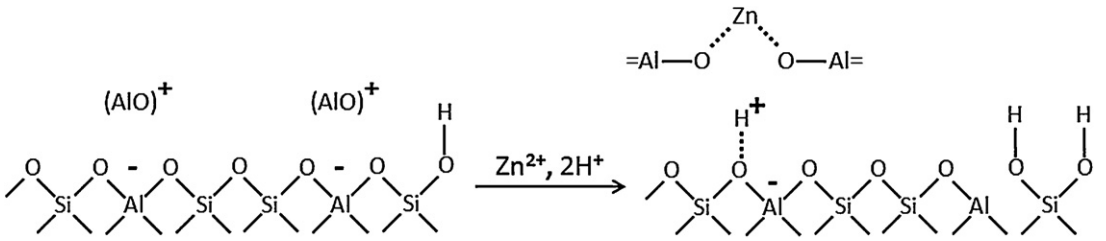

Scheme 1. Possible mechanism for the interaction of Zn^{2+} with extraframework aluminum on the surface of HBEA.

of zeolites. Grabienko et al. reported a decrease in the intensity of acidic hydroxyl groups at 3610 cm^{-1} on HBEA-54 due to the introduction of a Zn species [18]. Saberi et al. reported that the incorporated zinc species in Pt/HY behave as Lewis acid sites, which play an important role in the enhancement of isomerization activity [9], whereas Berndt et al. reported on the interaction of Zn with HZSM-5 in which the band of hydroxyl groups corresponding to extraframework aluminum at 3660 cm^{-1} was formed upon Zn loading with simultaneously decreasing bridging OH groups at 3610 cm^{-1} [36]. They concluded that the decrease in the intensity of the band at 3610 cm^{-1} indicated the interaction between Brønsted acid sites with Zn species, while the augmentation in the band at 3660 cm^{-1} indicated an increase in dislodged aluminum in the sample. Based on *in situ* X-ray absorption results, Biscardi et al. concluded that the interaction of $Zn(OH)^+$ with the surface of HZSM-5 varied depending on $Zn(OH)^+$ loading. At low $Zn(OH)^+$ loading, Zn^{2+} interacted with Si(OH)Al groups to form $Zn^{2+}(Si(O^-)Al)_2$, while at high $Zn(OH)^+$ loading, Zn^{2+} connected with another Zn^{2+} by bridging an O atom and two Zn^{2+} cations interacting with two Si(OH)Al groups to form $((Si(O^-)Al)Zn^{2+})_2O$ [20]. This result was also in agreement with our previous report for Zn/HZSM-5 in which Zn^{2+} interacted with Si(OH)Al to form strong Lewis acid sites and partially eliminated Brønsted acid sites [18].

FTIR spectroscopy was also employed to discriminate the states of hydroxyl groups and to identify the types of acid sites by recognizing the adsorption bonds formed between the acidic sites and probe molecules. The acidic character of HBEA and Zn-HBEA was observed using pyridine probe molecule FTIR spectroscopy. The band at 1545 cm^{-1} was assigned to C—N stretching of pyridinium ions ($C_5H_5NH^+$) bound to Brønsted acid sites on the zeolite surface, while the band at 1455 cm^{-1} was assigned to the vibration of physically adsorbed pyridine bound to Lewis acid sites. In this experiment, both HBEA and Zn-HBEA possessed Lewis and Brønsted acid sites after outgassing of adsorbed pyridine at 623 K, indicating that both samples possess relatively strong acid sites (Fig. 6). Generally, the Brønsted acid sites on zeolites are from tetrahedral structure of aluminum; however, the Brønsted acid sites in this HBEA are due to the presence of acidic hydroxyl groups (3660 cm^{-1}) corresponding to the presence of extraframework aluminum species $(AlO)^+$. In fact, no peak was observed at 3610 cm^{-1} assigned to bridging hydroxyl groups, Si(OH)Al, for the HBEA sample after high temperature calcination. The addition of Zn^{2+} to HBEA decreased Brønsted acid sites and increased Lewis acid sites. In addition, the presence of Zn^{2+} narrowed the strength distribution of Brønsted acid sites and widened the strength distribution of Lewis acid sites (Fig. 6B). The gradual increase in the strong and relatively weak Lewis acid sites was due to the presence Zn^{2+} cations which behave as new acidic centers in the HBEA. The decrease in the Brønsted acid sites was due to the elimination of $(AlO)^+$ acidic centers and the development of new acidic bridging hydroxyl groups, Si(OH)Al, in the aluminosilicate framework. The decrease in the number of hydroxyl groups corresponding to $(AlO)^+$ acidic centers was higher than that of the formation of Si(OH)Al acidic centers. Although it is not certain at present, it is plausible that two $(AlO)^+$ acidic centers interact with Zn^{2+} to form $Zn^{2+}(OAl=)_2$, leaving two OH hydroxyl groups and one Si(O—)Al in the framework. Then, Si(O—)Al is converted to an Si(OH)Al acidic center or an internal silanol group (non-acidic) and a coordinating Al^{3+} cation located in the extraframework Al-oxide cluster (Lewis acidic center). The formation of non-acidic internal silanol groups is in agreement with the formation of Q^2 sites in the NMR results and the shift of hydroxyl groups from 3740 cm^{-1} to 3745 cm^{-1}.

The characterization of acidic properties using pyridine adsorbed IR was done by Hedge et al. on the sodium and protonic forms BEA zeolites with an Si/Al ratio of 28 [37]. Both samples exhibited strong acidic sites after outgassing at 673 K. The absorbance bands were observed at 1546 and 1450 cm^{-1} which were assigned to pyridinium ions and pyridine molecules coordinated to protonic and Lewis acid sites on both samples, respectively. The protonation of sodium from BEA zeolite intensified the absorbance band at 1546 cm^{-1} and simultaneously decreased the number of acidic sites corresponding to Lewis acid sites at 1450 cm^{-1}. Grabienko et al. reported on the acidity of zeolite BEA based on CO adsorbed IR and ^1H MAS NMR analyses [17]. On the other hand, they reported that the band at 3740 cm^{-1}, ascribed to terminal silanol groups, indicates strong acidic silanol groups, similar to the band of SiOHAl groups at 3610 cm^{-1} according to the value of the low frequency shift of OH vibrations with adsorbed CO. The quantity of Si(OH)Al decreased with the loading of Zn; in contrast, there was no change when Ga was loaded on zeolite BEA.

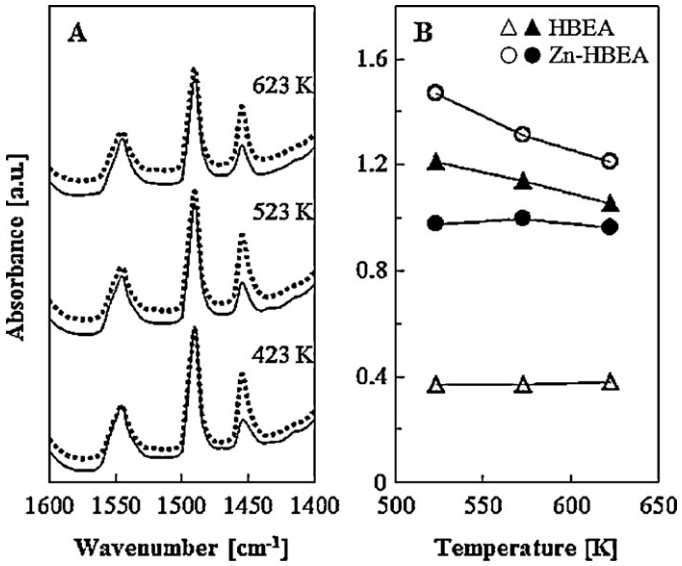

Fig. 6. (A) IR spectra of pyridine adsorbed HBEA (true lines) and Zn-HBEA (dotted lines). The samples were outgassed at 673 K for 3 h, followed by pyridine adsorption at 423 K and outgassing at 423 K, 523 K, and 623 K. (B) The changes in the intensities of Lewis and Brønsted acid sites against outgassing temperatures; (▲) HBEA; (●) Zn-HBEA; (white) Lewis acid site; (black) Brønsted acid site.

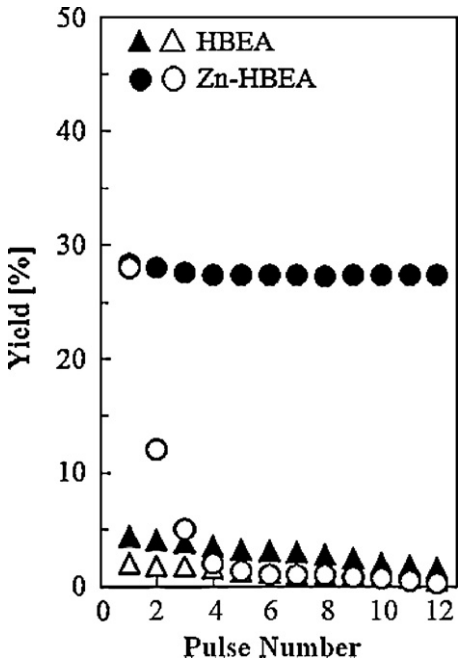

Fig. 7. Isomerization of *n*-pentane at 623 K over activated HBEA and Zn-HBEA in the presence of nitrogen (white) and hydrogen (black) gases. The catalysts were activated at 723 K under an oxygen stream for 30 min, followed by a hydrogen stream for 6 h.

3.2. Catalytic activity studies

Fig. 7 shows the activity of HBEA and Zn-HBEA in *n*-pentane isomerization under hydrogen and nitrogen streams at 623 K. Prior to the reaction, all samples were activated at 673 K under a hydrogen stream for 3 h. For the HBEA sample, the activity was less than 5% of the yield for isomerization under both hydrogen and nitrogen gases. The low activity of HBEA may be due to the absence of strong bridging hydroxyl groups and specific active sites which enhance isomerization. Zn-HBEA showed high activity and stability in *n*-pentane isomerization under hydrogen gas. The activity of Zn-HBEA decreased slightly in the initial reaction and reached steady state conditions within four pulse samplings (60 min) with the yield of isopentane at about 27%. In the presence of nitrogen gas, the high activity of Zn-HBEA decreased markedly from the initial reaction and was almost completely deactivated within four pulse samplings (60 min) of the reaction. The gradual decrease in the activity of Zn-HBEA may be due to the exhaustion of protonic acid sites on the surface of Zn-HBEA after starting the reaction under nitrogen gas. The absence of molecular hydrogen resulted in the inability of Zn-HBEA to regenerate and to maintain the active protonic acid sites on the surface of Zn-HBEA. Moreover, the accumulation of coke deposits on the surface could also be a major reason for the deactivation of Zn-HBEA.

Fig. 8 shows the effect of activation and reaction temperatures on *n*-pentane isomerization for the HBEA and Zn-HBEA samples. For the HBEA sample, trivial effects of activation and reaction temperatures were observed; however, the yield of isopentane did not exceed 5%. Nevertheless, the activity of Zn-HBEA changed significantly with the activation and reaction temperatures. Increasing the activation temperature removed relatively weak hydroxyl groups and formed strong Lewis acid sites in which the strong Lewis acid sites may be involved in the formation of active protonic acid sites for isomerization [16]. In addition, the activity of Zn-HBEA strongly depended on the reaction temperature (Fig. 8B). At 593 K and below, only a trace amount of isopentane was observed. Increasing the reaction temperature increased the activity of Zn-HBEA. The highest activity of Zn-HBEA was observed when the sample was activated at 723 K for 6 h and the reaction was carried out at 613 K, with isopentane being the main product and C_1—C_4 being the side products. No unsaturated and neopentane products were observed for all temperature range. The distribution of products is listed in Table 1. The apparent activation energies for HBEA and Zn-HBEA for reaction temperatures at 593–613 K were 118.76 and 90.79 kJ/mol, respectively (Fig. 9).

Several research groups have explored the modification of linear alkanes over modified zeolite BEA catalysts. Luzgin et al. [38]

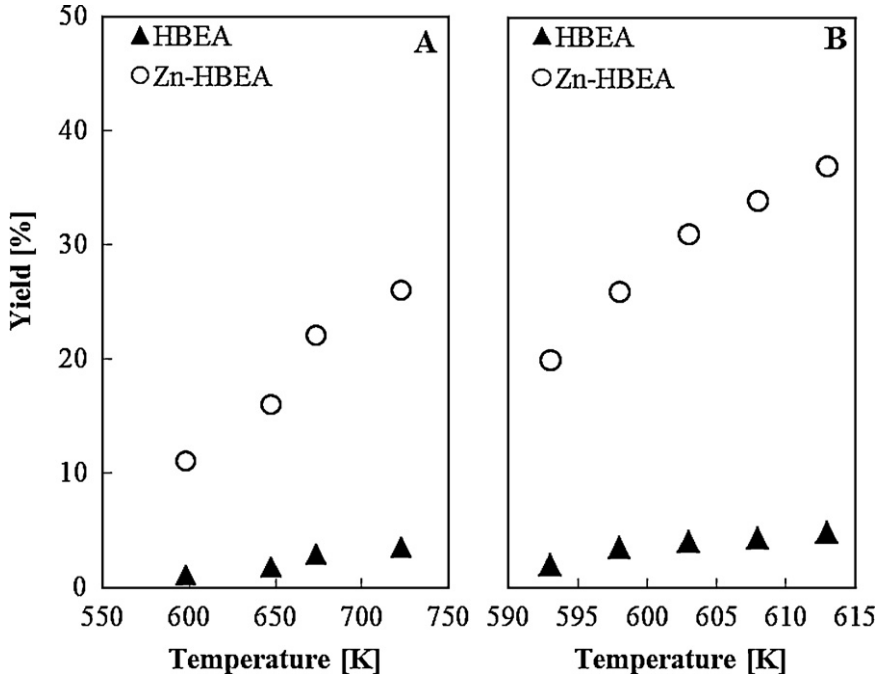

Fig. 8. (A) Effect of activation temperature on the isomerization of *n*-pentane at 598 K over Zn-HBEA. (B) Effect of reaction temperature on the isomerization of *n*-pentane over Zn-HBEA where the catalysts were activated at 723 K under a hydrogen stream for 6 h.

Table 1
Product distribution of *n*-pentane isomerization over HBEA and Zn-HBEA.

	Carrier gas	Treatment temperature (K)	Reaction temperature (K)	Conversion (%)	Selectivity (%)			Yield (%)
					C_1—C_2	C_3—C_4	iC_5	
Hβ	N_2	723	623	1.1	0.0	0.0	100.0	1.1
	H_2	723	623	7.6	38.0	19.9	42.1	3.2
Zn-Hβ	N_2	723	623	10.2	2.5	1.1	96.4	9.8
	H_2	723	623	31.3	9.8	5.2	85.0	26.6
	H_2	673	623	29.7	12.4	12.6	75.0	22.3
	H_2	648	623	27.5	18.7	21.3	60.0	16.5
	H_2	723	598	30.0	2.2	1.4	96.4	28.9
	H_2	723	648	42.0	25.6	24.4	50.0	21.0

and Arzumanov et al. [39] reported the use of Zn-modified zeolite BEA for the aromatization of low carbon number of linear alkanes. They concluded that a large quantity of evolved methane was produced, mainly by the direct hydrogenolysis of ethane, and aromatic products were provided by the alkylation reaction of methane with aromatics, which are produced exclusively from propane. Hydroisomerization of *n*-heptane over modified HBEA zeolite was reported by Liu et al. [26]. They concluded that the dealumination of HBEA with the loading of Pt together with Cr, Ce, La or Zn markedly increased the selectivity of isoheptane; the maximum selectivity of isoheptane and conversion of *n*-heptane were 97.0 and 65.5% over the CrPt/DBEA sample, respectively. Kusakari et al. [40] reported on the role of hydrogen and metal loading in *n*-pentane isomerization over a Pt/SiO_2–HBEA catalyst.

3.3. Formation and removal of coke deposits

Several research groups have reported on the effect of hydrogen carrier gas in the enhancement of the isomerization of linear alkanes. In general, it was concluded that hydrogen plays important roles in the formation of active sites in isomerization and the removal of coke deposits by hydrogenation [41]. Fig. 10 shows the *n*-pentane isomerization on Zn-HBEA; the carrier gas was sequentially switched from hydrogen to nitrogen and back to hydrogen. In the first reaction under hydrogen gas, the selectivity of isopentane and the conversion of *n*-pentane reached 96.4 and 30.0%, respectively. However, the selectivity decreased markedly to less than 10% and the conversion was close to zero after the hydrogen carrier gas was switched to nitrogen. This decrease in the catalytic activity after switching the carrier gas to nitrogen may have been due to the gradual exhaustion of protonic acid sites on the surface of the Zn-HBEA and the formation of coke deposits on the surface. The presence of hydrogen in the gas phase is required to provide and maintain active protonic acid sites in isomerization. The activity of Zn-HBEA recovered slowly when the carrier gas was switched back to hydrogen. Although the activity did not recover completely after switching back to hydrogen, a promoting effect of hydrogen was observed on the Zn-HBEA catalyst. Minor deactivation of Zn-HBEA may be caused by the presence of coke deposits on the surface of Zn-HBEA which cannot be removed during the reaction.The presence of coke deposits during the reaction under a nitrogen stream was observed by IR spectroscopy and TGA analyses. Fig. 11 shows the IR spectra of fresh Zn-HBEA and used Zn-HBEA catalysts under hydrogen and nitrogen gases. Coked Zn-HBEA shows the development of several bands at 1405, 1460, 1470, 1485, 1501, 1530, 1560, 1575, and 1645 cm^{-1}. The bands at 1405 and 1460 cm^{-1} are attributed to branched alkanes, while the band at 1470 cm^{-1} corresponds to the rocking and bending vibration of $-CH_2$ [42,43].

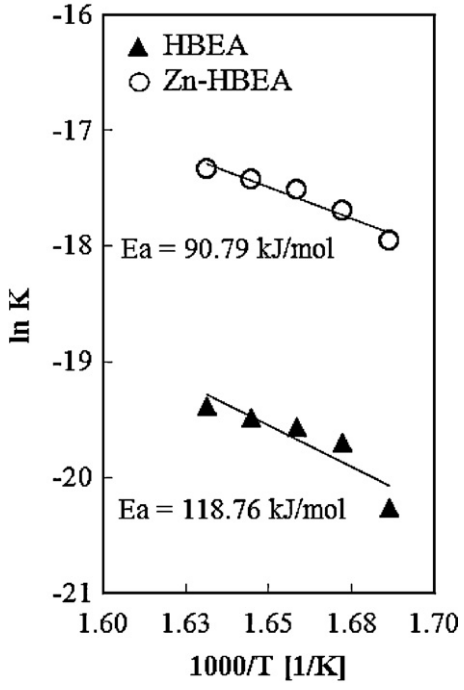

Fig. 9. Arrhenius plot for *n*-pentane isomerization over HBEA and Zn-HBEA in the temperature range of 373–648 K.

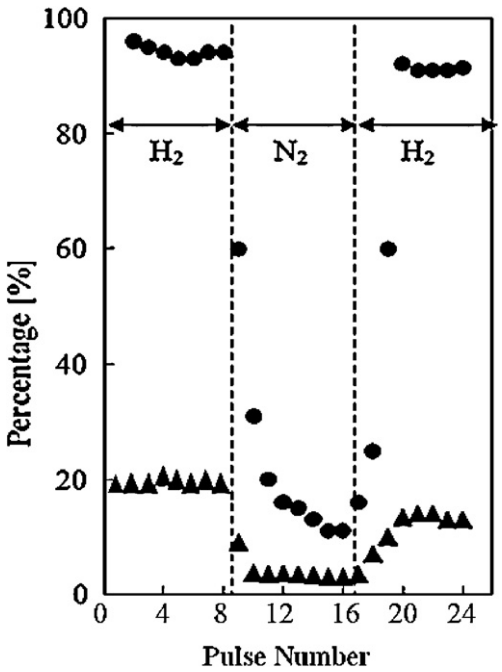

Fig. 10. Conversion of *n*-pentane (▲) and selectivity of isopentane (●) over Zn-HBEA at 623 K under hydrogen and nitrogen streams.

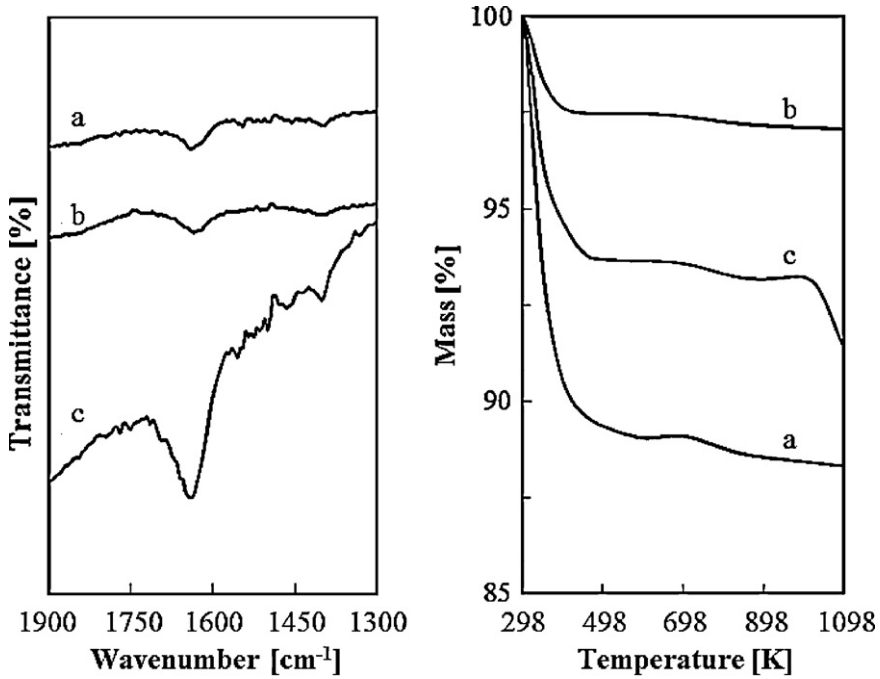

Fig. 11. (A) FTIR spectra of Zn-HBEA; (a) fresh catalyst, (b) after isomerization in the presence of hydrogen and (c) after isomerization in the presence of nitrogen. (B) TGA plot for Zn-HBEA; (a) fresh catalyst, (b) after the isomerization in the presence of hydrogen and (c) after the isomerization in the presence of nitrogen.

The band at 1485 cm^{-1} is associated with deformation vibration of the C—H bond of adsorbed olefins, which indicates that a substantial amount of coke and carbonaceous species formed in the absence of H_2 [44]. The band at 1501 cm^{-1} is assigned to C—C vibration of alkyl carbenium ions, while the strong distinctive band at 1645 cm^{-1} is related to the C=C bond, indicating the presence of olefinic species, which were inhibited from undergoing further conversion and were deposited as coke [44]. TGA analysis confirmed the formation of coke deposits on used Zn-HBEA (N_2). About 4% of the mass was desorbed at 998 K which may be related to heavy coke deposits from linear alkanes on the sample surface. Although we do not have a plausible mechanism for the formation of coke deposits on the Zn/HBEA at present, coke is most probably deposited in the internal surface of zeolite intimately associated with the active sites of the zeolite [45].

4. Conclusion

Electrodeposition and ion exchange methods were used to produce Zn^{2+} cations and introduce Zn^{2+} cations into an HBEA sample. The presence of Zn^{2+} cations did not considerably change the crystallinity, specific surface area and pore distribution of HBEA. The Zn^{2+} cations interacted with $(AlO)^+$ extraframework aluminum to form $Zn(OAl=)_2$ and Si(OH)Al. The $(AlO)^+$ extraframework aluminum acidic center was eliminated and a new bridging hydroxyl group acidic center, Si(OH)Al, was developed. The formation of $Zn(OAl=)_2$ on the sample surface increased the acidic centers for Lewis acid sites. In addition, the addition of Zn^{2+} narrowed the distribution of Brønsted acid sites and widened the distribution of Lewis acid sites.

The activity of the HBEA sample for *n*-pentane isomerization was increased by loading Zn^{2+} cations due to the increase in strong Lewis acid sites which may facilitate the formation of active protonic acid sites from molecular hydrogen through a hydrogen spillover mechanism. The presence of Zn^{2+} cations also stabilized the activity and suppressed the formation of coke deposits on the surface by a hydrogenation process.

Acknowledgement

This work was supported by The Ministry of Higher Education, Malaysia through the Fundamental Research Grant Scheme (No. 78670). Our gratitude also goes to the Hitachi Scholarship Foundation for the Gas Chromatograph Instruments Grant.

References

[1] S. Gopal, P.G. Smirniotis, Appl. Catal. A: Gen. 247 (2003) 113–123.
[2] S. Triwahyono, A.A. Jalil, H. Hattori, J. Nat. Gas Chem. 16 (2007) 252–257.
[3] H. Liu, G.D. Lei, W.M.H. Sachtler, Appl. Catal. A: Gen. 137 (1996) 167–177.
[4] S. Zhang, S.L. Chen, P. Dong, G. Yuan, K. Xu, Appl. Catal. A: Gen. 332 (2007) 46–55.
[5] G. Wang, Q. Liu, W. Su, X. Li, Z. Jiang, X. Fang, C. Han, C. Li, Appl. Catal. A: Gen. 247 (2003) 113–123.
[6] A.K. Aboul-Gheit, A.E. Awadallah, N.A.K. Aboul-Gheit, E.-S.A. Solyman, M.A. Abdel-Aaty, Appl. Catal. A: Gen. 334 (2008) 304–310.
[7] H.D. Setiabudi, A.A. Jalil, S. Triwahyono, N.H.N. Kamarudin, R.R. Mukti, Appl. Catal. A: Gen. 417–418 (2012) 190–199.
[8] P. Liu, X. Zhang, Y. Yao, J. Wang, Appl. Catal. A: Gen. 371 (2009) 142–147.
[9] M.A. Saberi, R. Le Van Mao, M. Martin, A.W.H. Mak, Appl. Catal. A: Gen. 214 (2001) 229–236.
[10] M.A.A. Aziz, N.H.N. Kamarudin, H.D. Setiabudi, H. Hamdan, A.A. Jalil, S. Triwahyono, J. Nat. Gas Chem. 21 (2012) 29–36.
[11] R.C.R. Santos, A. Valentini, C.L. Lima, J.M. Filho, A.C. Oliveira, Appl. Catal. A: Gen. 403 (2011) 65–74.
[12] S. Triwahyono, T. Yamada, H. Hattori, Catal. Lett. 85 (2003) 109–115.
[13] N.N. Ruslan, N.A. Fadzlillah, A.H. Karim, A.A. Jalil, S. Triwahyono, Appl. Catal. A: Gen. 406 (2011) 102–112.
[14] N.N. Ruslan, S. Triwahyono, A.A. Jalil, S.N. Timmiati, N.H.R. Annuar, Appl. Catal. A: Gen. 413–414 (2012) 176–182.
[15] H.D. Setiabudi, S. Triwahyono, A.A. Jalil, N.H.N. Kamarudin, M. Arif, A. Aziz, J. Nat. Gas Chem. 20 (2011) 477–482.
[16] S. Triwahyono, A.A. Jalil, M. Musthofa, Appl. Catal. A: Gen. 372 (2010) 90–93.
[17] A.A. Gabrienko, I.G. Danilova, S.S. Arzumanov, A.V. Toktarev, D. Freude, A.G. Stepanov, Microporous Mesoporous Mater. 131 (2010) 210–216.
[18] A.G. Stepanov, S.S. Arzumanov, A.A. Gabrienko, A.V. Toktarev, V.N. Parmon, D. Freude, J. Catal. 253 (2008) 11–21.
[19] V.B. Kazansky, in: G. Ohlmann, H. Pfeifer, R. Fricke (Eds.), Catalysis and Adsorption by Zeolites, Elsevier Science Publishers, Amsterdam, 1991, pp. 117–131.
[20] J.A. Biscardi, G.D. Meitzner, E. Iglesia, J. Catal. 179 (1998) 192–202.
[21] S. Triwahyono, A.A. Jalil, R.R. Mukti, M. Musthofa, N. Aini, M. Razali, M. Arif, A. Aziz, Appl. Catal. A: Gen. 407 (2011) 91–99.
[22] A.A. Jalil, N. Kurono, M. Tokuda, Synlett 12 (2001) 1944–1946.
[23] S. Triwahyono, Z. Abdullah, A.A. Jalil, J. Nat. Gas Chem. 15 (2006) 247–252.

[24] J.B. Higgins, R.B. LaPierre, J.L. Schlenker, A.C. Rohrman, J.D. Wood, G.T. Kerr, W.J. Rohrbaugh, Zeolites 8 (1998) 446–452.
[25] J.P. Pariente, G. Pal-Borbely, J.A. Martens, P.A. Jacobs, Appl. Catal. A: Gen. 31 (1987) 35–46.
[26] P. Liu, J. Wang, X. Zhang, R. Wei, X. Ren, Chem. Eng. J. 148 (2009) 184–190.
[27] R. Kumar, A. Thangaraj, R.N. Bhat, P. Ratnasamy, Zeolites 10 (1990) 85–89.
[28] H.K. Beyer, M. Keindl, Microporous Mesoporous Mater. 31 (1999) 333–341.
[29] Y. Ni, A. Sun, X. Wu, G. Hai, J. Hu, T. Li, G. Li, Microporous Mesoporous Mater. 143 (2011) 435–442.
[30] K.S.W. Sing, Adv. Colloid Interface Sci. 76–77 (1989) 3–11.
[31] X. Xiang, X.T. Zu, S. Zhu, C.F. Zhang, L.M. Wang, Nucl. Instrum. Methods Phys. Res. 250 (2006) 192–195.
[32] J. Klinowski, Colloids Surf. 36 (1989) 133–154.
[33] M. Hunger, E. Brunner, Mol. Sieves 4 (2004) 201–293.
[34] G.P. Heitmann, G. Dahlhoff, W.F. Hoelderich, Appl. Catal. A: Gen. 185 (1999) 99–108.
[35] J.A. Lercher, A. Jentys, in: J. Cejka, H. van Bekkum, A. Corma, F. Schuth (Eds.), Introduction to zeolite science and practise, 3rd revised edition, Elsevier, Amsterdam, 2007, p. 452.
[36] H. Berndt, G. Lietz, B. Lucke, J. Volter, Appl. Catal. A: Gen. 146 (1996) 351–363.
[37] S.G. Hedge, R. Kumar, R.N. Bhat, P. Ratnasamy, Zeolites 9 (1989) 231–237.
[38] M.V. Luzgin, V.A. Rogov, S.S. Arzumanov, A.V. Toktarev, A.G. Stepanov, V.N. Parmon, Catal. Today 144 (2009) 265–272.
[39] S.S. Arzumanov, A.A. Gabrienko, D. Freude, A.G. Stepanov, Solid State Nucl. Magn. Reson. 35 (2009) 113–119.
[40] T. Kusakari, K. Tomishige, K. Fujimoto, Appl. Catal. A: Gen. 224 (2002) 219–228.
[41] Y.C. Yang, H.S. Weng, J. Mol. Catal. A 304 (2009) 65–70.
[42] A. Lucas, R. Canizares, A. Durfin, A. Carrero, Appl. Catal. A: Gen. 156 (1997) 299–317.
[43] M.S. Renzini, L.C. Lerici, U. Sedran, L.B. Pierella, J. Anal. Appl. Pyrolysis 92 (2011) 450–455.
[44] J.N. Kondo, S. Yang, Q. Zhu, S. Inagaki, K. Domen, J. Catal. 248 (2007) 53–59.
[45] D.M. Bibby, N.B. Milestone, J.E. Patterson, L.P. Aldridge, J. Catal. 97 (1986) 493–502.